# Proton-Coupled Structural Changes upon Binding of Carbon Monoxide to Cytochrome $cd_1$: A Combined Flash Photolysis and X-ray Crystallography Study[†,‡]

Tove Sjögren,[§,||] Margareta Svensson-Ek,[§,||] Janos Hajdu,*[,§] and Peter Brzezinski*[,⊥]

*Department of Biochemistry, Uppsala University, Biomedical Center, Box 576, SE-751 23 Uppsala, Sweden, and Department of Biochemistry, The Arrhenius Laboratories for Natural Sciences, Stockholm University, SE-106 91 Stockholm, Sweden*

*Received January 31, 2000; Revised Manuscript Received May 1, 2000*

ABSTRACT: We have investigated dynamic events after flash photolysis of CO from reduced cytochrome $cd_1$ nitrite reductase (NiR) from *Paracoccus pantotrophus* (formerly *Thiosphaera pantotropha*). Upon pulsed illumination of the cytochrome $cd_1$−CO complex, at 460 nm, a rapid (<50 ns) absorbance change, attributed to dissociation of CO, was observed. This was followed by a biphasic rearrangement with rate constants of $1.7 \times 10^4$ and $2.5 \times 10^3$ $s^{-1}$ at pH 8.0. Both parts of the biphasic rearrangement phases displayed the same kinetic difference spectrum in the region of 400−660 nm. The slower of the two processes was accompanied by proton uptake from solution (0.5 proton per active site at pH 7.5−8.5). After photodissociation, the CO ligand recombined at a rate of 12 $s^{-1}$ (at 1 mM CO and pH 8.0), accompanied by proton release. The crystal structure of reduced cytochrome $cd_1$ in complex with CO was determined to a resolution of 1.57 Å. The structure shows that CO binds to the iron of the $d_1$ heme in the active site. The ligation of the *c* heme is unchanged in the complex. A comparison of the structures of the reduced, unligated NiR and the NiR−CO complex indicates changes in the puckering of the $d_1$ heme as well as rearrangements in the hydrogen-bonding network and solvent organization in the substrate binding pocket at the $d_1$ heme. Since the CO ligand binds to heme $d_1$ and there are structural changes in the $d_1$ pocket upon CO binding, it is likely that the proton uptake or release observed after flash-induced CO dissociation is due to changes of the protonation state of groups in the active site. Such proton-coupled structural changes associated with ligand binding are likely to affect the redox potential of heme $d_1$ and may regulate the internal electron transfer from heme *c* to heme $d_1$.

Bacterial denitrification serves an important role in cellular bioenergetics and the global nitrogen cycle. It is performed by a series of oxidoreductases which constitute a respiratory chain in which nitrogen oxyanions and oxides are used as electron acceptors (*1*, *2*). Cytochrome $cd_1$ nitrite reductase (NiR)[1] is one of the enzymes involved in denitrification. Its physiological role is to catalyze the one-electron reduction of nitrite to nitric oxide:

$$NO_2^- + e^- + 2H^+ \rightarrow NO + H_2O \qquad (1)$$

In addition, it can also catalyze the four-electron reduction of oxygen to water, and has thus been known as a soluble cytochrome oxidase. The three-dimensional structure of oxidized NiR from *Paracoccus pantotrophus* [formerly known as *Thiosphaera pantotropha* LMD 92.63 (*3*)] has been determined to high resolution (*4*, *5*). The soluble periplasmic protein is a homodimer with a subunit molecular mass of 60 kDa. Each subunit is divided into two domains. The N-terminal part forms a cytochrome *c*-like domain containing a *c* heme. The *c* heme has an unusual His-His ligation (His17 and His69 in *P. pantotrophus*) in the oxidized state but undergoes a His-Met ligand switching (His69 and Met106) upon reduction in the crystal (*6*). The C-terminal part forms an eight-bladed $\beta$-propeller structure containing a noncovalently bound $d_1$ heme. The $d_1$ heme is the site of nitrite and oxygen reduction. This heme is hexacoordinated in the oxidized state with His200 and Tyr25 as axial ligands, and pentacoordinated in the reduced state, when Tyr25 is released from the active site. Heme *c* is the site of electron entry from external electron donors such as pseudoazurin or cytochrome $c_{551}$ (*1*, *2*, *7*, *8*). The electron is then transferred internally to the $d_1$ heme, where catalysis takes place. Cytochrome $cd_1$ from *P. pantotrophus* was the first heme-containing nitrite reductase whose structure was determined (*4*, *5*), but many of the functional and kinetic studies were performed on another cytochrome $cd_1$ NiR, the enzyme from *Pseudomonas aeruginosa* (*9*−*12*). There is now a growing body of evidence which shows that, despite many similarities, certain functional properties of the two enzymes are fundamentally

[†] Supported by grants to P.B. from the Swedish Natural Science Research Council and The Swedish Foundation for International Cooperation in Research and Higher Education (STINT) and to J.H. from the Swedish Natural Science Research Council and EU-BIOTECH (BIO4-CT96-0281 and BIO4-CT98-0415).

[‡] The coordinates have been deposited as PDB entry 1DY7.

* To whom correspondence should be addressed. P.B.: Department of Biochemistry, The Arrhenius Laboratories for Natural Sciences, Stockholm University, SE-106 91 Stockholm, Sweden; e-mail, peterb@biokemi.su.se; fax, (+46)-8-153679. J.H.: Department of Biochemistry, Uppsala University, Biomedical Center, Box 576, SE-751 23 Uppsala, Sweden, e-mail, janos@xray.bmc.uu.se; fax, (+46)-18-511755.

[§] Uppsala University.

[||] These authors have contributed equally to this work.

[⊥] Stockholm University.

[1] Abbreviation: NiR, nitrite reductase.

10.1021/bi000179q CCC: $19.00 
Published on Web 08/12/2000

different (*13*, *14*, *32*; M. Svenson-Ek et al., unpublished). A comparison of the structures of cytochromes $cd_1$ from *Ps. aeruginosa* (*15*) and *P. pantotrophus* (*4*) shows that the enzymes display differences in their heme ligation in the oxidized state. While in the *P. pantotrophus* enzyme heme *c* has His-His ligation (cf. above), the *Ps. aeruginosa* enzyme has His-Met ligation similar to the reduced form of the *P. pantotrophus* $cd_1$ NiR. In addition, while the sixth $d_1$ heme ligand in the *P. pantotrophus* enzyme is a tyrosine (Tyr25), the corresponding ligand in the *Ps. aeruginosa* enzyme is a water molecule linked to a tyrosine (Tyr10, *Ps. aeruginosa* amino acid numbering) by a hydrogen bond. Furthermore, an N-terminal arm exchange has been observed in the *Ps. aeruginosa* enzyme (*15*). It has been suggested that Tyr25 in the *P. pantotrophus* NiR may be important for blocking the $d_1$ heme under oxidative stress (*6*), but it may also play an active part in nitrite reduction by facilitating release of the product from the $d_1$ heme (*2*, *4*, *6*, *32*). Mutagenesis of the corresponding residue in the *Ps. aeruginosa* NiR (Tyr10) does not affect activity. Optical absorption spectra and studies on the electron-transfer kinetics of the enzyme (*16*) further support the view that the Tyr10 is not necessary for catalysis in the *Ps. aeruginosa* enzyme.

The observed differences in the structural and functional properties of the *P. pantotrophus* and *Ps. aeruginosa* enzymes call for further studies. In this paper, we investigate the properties of the substrate-binding site in the *P. pantotrophus* NiR, following laser-induced dissociation of CO from the $d_1$ heme iron of reduced cytochrome $cd_1$ NiR. The electronic properties of carbon monoxide show certain similarities to the electronic properties of nitric oxide (a product) and dioxygen (a substrate). All three ligands bind to the $d_1$ heme in cytochrome $cd_1$ (*9*). The bond between CO and the iron of heme $d_1$ is photolabile, and the CO ligand can thus be photodissociated from the enzyme. This phenomenon can be exploited in kinetic studies for the rapid trigger of catalysis or for probing the structural plasticity and dynamics of the active site. Our results demonstrate that flash photolysis of the enzyme−CO complex in solution is followed by two rapid kinetic phases similar to those reported for the *Ps. aeruginosa* enzyme (*17*). In the study presented here, we found that in the *P. pantotrophus* enzyme the slower of these phases is correlated with proton uptake. On the basis of the three-dimensional structure of the reduced enzyme and the reduced CO complex, we suggest a possible mechanism for this reaction and for the rearrangement phases following CO dissociation. Furthermore, since the reduced heme $d_1$ forms a very tight complex with NO, we speculate that proton uptake (i.e., a net increase in the number of positive charges in the active site area) may have a regulatory role following ligand dissociation in facilitating electron transfer to an empty heme $d_1$.

## MATERIALS AND METHODS

*Enzyme Purification. P. pantotrophus* cytochrome $cd_1$ nitrite reductase was purified as described by Moir et al. (*7*). After purification, the enzyme was concentrated to 0.5 mM in 50 mM potassium phosphate buffer (pH 7.0) and stored at −70 °C.

*Preparation of the Enzyme−CO Complex.* An enzyme solution was transferred into an airtight 3 mL, four-window fluorescence cuvette (10−20 $\mu$M with respect to the 60 kDa monomer; for details, see the figure legends). The cuvette was repetitively evacuated on a vacuum line and flushed with nitrogen. To reduce the enzyme, ascorbate and phenazine methosulfate (PMS) were added anaerobically to final concentrations of 1 mM and 5 $\mu$M, respectively. After reduction, nitrogen was exchanged for carbon monoxide at 1 atm, which resulted in formation of the cytochrome $cd_1$−CO complex.

*Flash Photolysis Studies.* The CO ligand was photodissociated with a 10 ns, ∼100 mJ laser flash at 532 nm (Nd:YAG laser, Spectra Physics). The reaction was followed spectroscopically at several wavelengths in the 400−660 nm range. Care was exercised to keep the measuring light intensity at a low level to prevent dissociation of CO prior to the laser flash. The cuvette path length was 1.00 cm. The observation equipment has been described in detail elsewhere (*18*, *19*).

*Measurements of the Thermal CO Dissociation Kinetics.* A solution of ascorbate-reduced NiR with CO bound to heme $d_1$ was prepared in an anaerobic cuvette as described above and transferred anaerobically to one of the drive syringes of a locally modified stopped-flow apparatus (Applied Photophysics, DX-17MV). The other syringe was filled with a buffer solution equilibrated with $O_2$. The mixing ratio of the enzyme and $O_2$ solutions was 1:5, giving CO and $O_2$ concentrations of ∼170 $\mu$M and ∼1 mM, respectively, after mixing. The temperature of the sample compartment was controlled by a flow of anaerobic, thermostated water around the cuvette and drive syringes.

*Measurements of Changes in the Protonation State after Flash-Induced CO Dissociation.* The enzyme stock was diluted to 10 $\mu$M with 0.1 M KCl, adjusted to pH 7 with KOH, and reconcentrated and diluted until negligible amounts of buffer remained (>3000-fold dilution) using Centricon-10 concentrator tubes (Amicon). A pH-indicator dye (phenol red at pH 7.5 and cresol red at pH 8.5) at a concentration of 40 $\mu$M was added to the enzyme solution. The enzyme−CO complex was prepared as described above, and the pH was adjusted after reduction. Photolysis experiments were performed as described previously (*18*, *19*). To determine the buffer capacity of the sample, the cuvette was placed in a spectrophotometer (Cary 4, Varian), and small volumes (5−10 $\mu$L to 1.5 mL of enzyme solution) of an anaerobic solution of HCl were then added. Each addition resulted in an approximate increase in proton concentration of 6 $\mu$M. The $\Delta A/H^+$ was determined from an average value of four to five additions. After the buffer capacity was determined, an anaerobic, concentrated buffer solution was added to the sample at the same pH as the unbuffered one, and the CO recombination kinetics was measured again. Absorbance changes associated with changes in the protonation state of the enzyme were determined by subtracting the signal obtained with the buffered solution from that obtained with the unbuffered one.

The amount of reacting enzyme was determined from the CO dissociation absorbance change at 460 nm, using an absorption coefficient of 20 $mM^{-1}$ $cm^{-1}$ for the reduced enzyme (*20*).

*Determination of the Structure of the Reduced Cytochrome $cd_1$−CO Complex.* Crystals of oxidized cytochrome $cd_1$ were obtained as described previously (*21*) and were reduced with

Table 1: X-ray Data Collection and Refinement Statistics

| | |
|---|---|
| **Data Collection** | |
| space group | $P2_1$ |
| cell dimensions | $a = 106.9$ Å, $b = 61.0$ Å, $c = 100.4$ Å, $\beta = 111.8°$ |
| no. of molecules in asymmetric unit | one dimer |
| resolution range (Å) (outer shell) | 30−1.57 (1.64−1.57) |
| no. of reflections | 148443 |
| *R*-merge (%) (outer shell) | 4.0 (17) |
| completeness (%) (outer shell) | 87.6 (83.7) |
| **Statistics for the Final Model** | |
| no. of residues | 976 [134−567 (subunit A), 26−567 (subunit B)] |
| no. of solvent molecules | 856 (851 water molecules, 3 sulfate ions, 2 glycerol molecules) |
| *R*-factor (%) | 17.8 |
| free *R*-factor (%) | 19.9 |
| average *B*-factor, protein atoms (Å$^2$) | 16.5 |
| average *B*-factor, all atoms (Å$^2$) | 17.5 |
| *B*-factor for C in CO (Å$^2$) | 17.4 (subunit A), 14.8 (subunit B) |
| *B*-factor for O in CO (Å$^2$) | 20.1 (subunit A), 19.4 (subunit B) |
| rmsd for bond lengths (Å) | 0.017 |
| rmsd for bond angles (deg) | 1.4 |

dithionite according to the method of Williams et al. (*6*). The reduced crystals were incubated under 15 atm of CO for 20 min at −20 °C, using a pressure cell (4DX Systems AB, Uppsala, Sweden) to obtain the enzyme−CO complex in the protein crystal. Data to a resolution of 1.57 Å were collected at 100 K using monochromatic X-rays at a wavelength of 0.935 Å on beam line ID14 at the European Synchrotron Radiation Facility (ESRF) in Grenoble, France. The refined model of the reduced protein was used for initial phasing (*6*). The phases were refined using the REFMAC (*22*) program, and model building was done with O (*23*). The asymmetric unit of the $P2_1$ crystals contains a dimer, and therefore, the environment of the two chemically identical subunits is different in the crystal lattice. One of the cytochrome *c* domains (subunit A) was highly disordered in the crystal and could not be refined. However, the cytochrome *c* domain of the B subunit and both $d_1$ domains could be refined without difficulties. The overall crystallographic *R*-factor for the final model was 17.7%, and the free *R*-factor was 19.9% (Table 1).

## RESULTS

*Structure of the Reduced Enzyme Complexed with CO.* The structure of the reduced *P. pantotrophus* cytochrome $cd_1$ NiR−CO complex was determined to a resolution of 1.57 Å. The overall structure is similar to that of the reduced enzyme (*6*) with a rmsd of 0.5 Å when all Cα atoms of the three ordered domains are superimposed. CO binds to the $d_1$ heme in the active site (Figure 1A) with an Fe−C bond length of 1.9 Å and an Fe−C−O angle of 158°. In pentacoordinated model heme *b* complexes, the Fe−C−O geometry is approximately linear (*24*, *25*), although calculations show that bending of the Fe−C−O bond by less than 25° results in very small energetic differences (*26*). His388 $N_\epsilon$ occupies a position above the $d_1$ heme iron, imposing a sterical restraint on the bound CO molecule. This explains the 22° deviation from linearity in the Fe−C−O bond angle. An additional factor is that the $d_1$ heme is not continuously conjugated.

The partially saturated porphyrin ring of the $d_1$ heme is distorted from planarity in the structure of reduced NiR (*6*). In the reduced NiR−CO complex, this distortion is even more pronounced, bringing the carboxyl groups of the porphyrin ring closer together (Figure 1A,D). This may affect the p*K* of these moieties. In the reduced NiR structure, a water molecule is located between residues His345 and His388 above the plane of the $d_1$ heme (Figure 1D). This water is displaced by approximately 1 Å when carbon monoxide binds to the $d_1$ heme of the reduced enzyme (W252, Figure 1A). The oxygen atom of CO makes a hydrogen bond to this water molecule and also to the $N_\epsilon$ atom of His388 (Figure 1A). W252 is linked to a chain of three other water molecules leading to the surface, constituting a possible proton/substrate/product transfer pathway (Figure 1B).

Nitric oxide has been shown to be able to bind in two different conformations, one which is similar to the CO conformation (see Figure 1C) and the other where the oxygen atom of NO is located between His388 and His345 (*6*; see also ref *32*). Quantum mechanical calculations show that the latter conformation is the more stable one (*32*). However, NO binds to the $d_1$ heme with a greater tilt angle than CO. This conformation is energetically unfavorable for CO, as it would require a substantial bending of the Fe−C−O bond.

*CO Recombination Kinetics following Pulsed Illumination.* Figure 2 shows the optical absorption spectra of the oxidized, reduced, and the reduced carbon monoxide complex of the *P. pantotrophus* cytochrome $cd_1$ nitrite reductase (NiR). Carbon monoxide binds to reduced cytochrome $cd_1$ NiR, and the binding is associated with changes in the absorption spectrum mainly in regions correlated with the electronic environment of the $d_1$ heme (Figure 2 and ref *13*).

The heme $d_1$−CO bond is photolabile, and the CO ligand can thus be photodissociated from the enzyme with a short laser flash. Panels A and B of Figure 3 show absorbance changes at 460 nm associated with flash-induced dissociation and recombination of CO under anaerobic conditions. The rapid (<50 ns) increase in absorbance at 460 nm was followed by biphasic rearrangement of the enzyme (Figure 3A), and on a longer time scale by a slower decrease in absorbance associated with CO recombination (Figure 3B). At 1 mM CO, the CO recombination rate ($k_{on}$) was $13 \pm 1$ $s^{-1}$. This rate was essentially independent of pH in the range of 5.5−8.5 ($13 \pm 2$ $s^{-1}$). The second-order rate constant of the CO recombination was estimated to be $\sim 1.3 \times 10^4$ $M^{-1}$ $s^{-1}$.

Curve 1 in Figure 3C shows the kinetic difference spectrum[2] observed during recombination of CO with reduced cytochrome $cd_1$, following flash photolysis of the NiR−CO complex. Curve 2 of this figure shows the static difference spectrum between the reduced enzyme complexed with CO and the unliganded reduced enzyme. The kinetic difference spectrum (curve 1 in Figure 3C) and the static difference spectrum (curve 2 in Figure 3C) exhibit identical features, indicating that the $\sim 13$ $s^{-1}$ phase was due to CO recombination.

*Rapid Rearrangement following Dissociation of CO.* When measured on a shorter time scale, a biphasic absorbance change with rate constants of $(2.2 \pm 0.7) \times 10^4$ and $(4.0 \pm 0.1) \times 10^3$ $s^{-1}$ (SD of 11 measurements) at pH 8.0 was

[2] The term "kinetic difference spectrum" refers to the difference in absorbance at $t \rightarrow \infty$ and $t = 0$ for a kinetic phase.

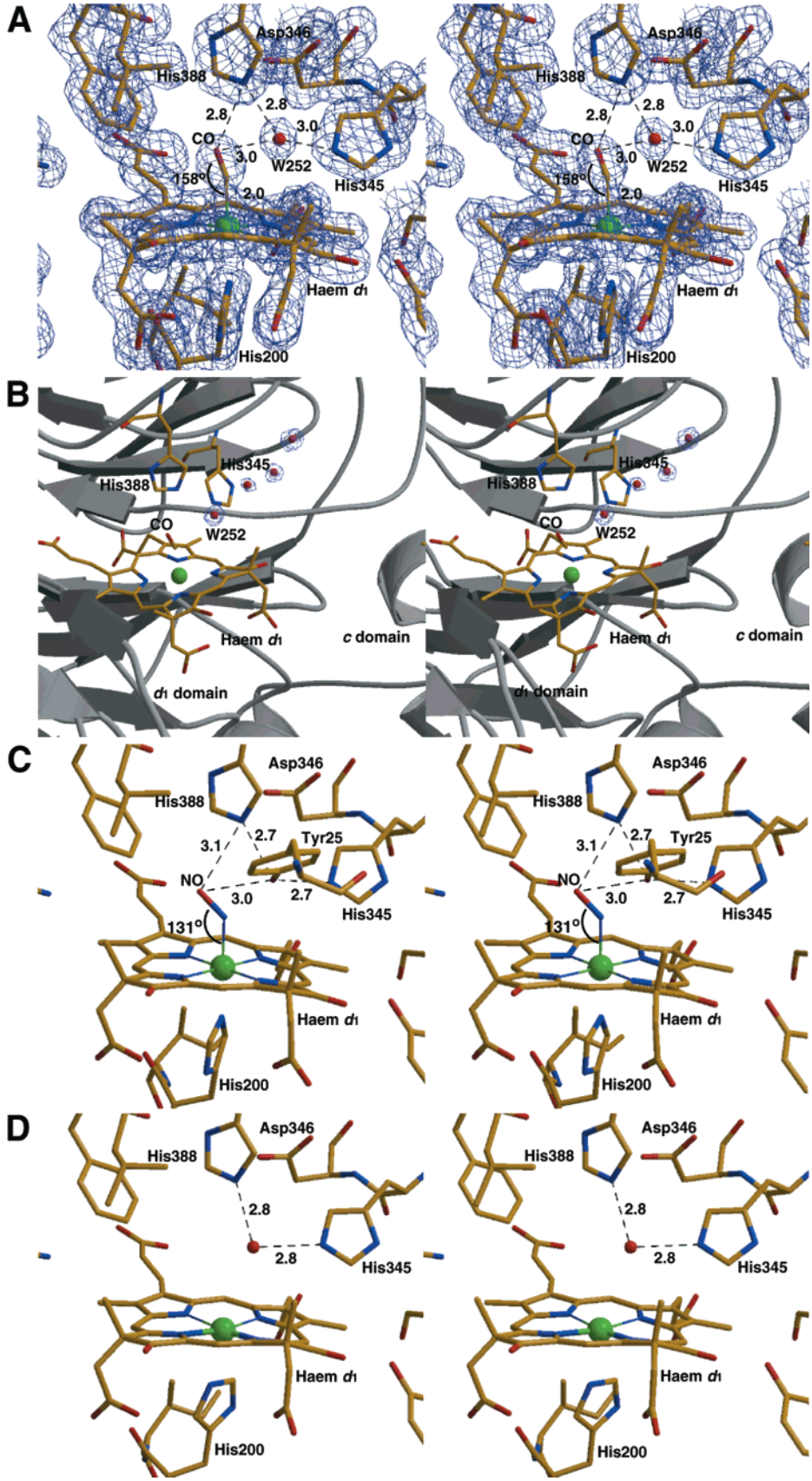


FIGURE 1: Stereoviews of the structure of reduced cytochrome $cd_1$ nitrite reductase complexed with carbon monoxide compared to the structure of the reduced enzyme and the structure of the oxidized enzyme in complex with NO. The $2F_{obs} - F_{calc}$ electron density maps were contoured at $1.5\sigma$, where $\sigma$ is the root-mean-square electron density for the unit cell. (A) The active site $d_1$ heme with CO bound at 1.57 Å resolution. (B) The chain of water molecules leading from the active site to the surface of this complex. (C) The structure of the NO complex of oxidized cytochrome $cd_1$ (PDB entry 1AOM) (*6*). (D) The structure of the unliganded reduced enzyme obtained through reduction with methyl viologen (*6*). Figures were drawn using the program Molscript (*30*), modified by R. Esnouf, and rendered using the program Raster3D (*31*).

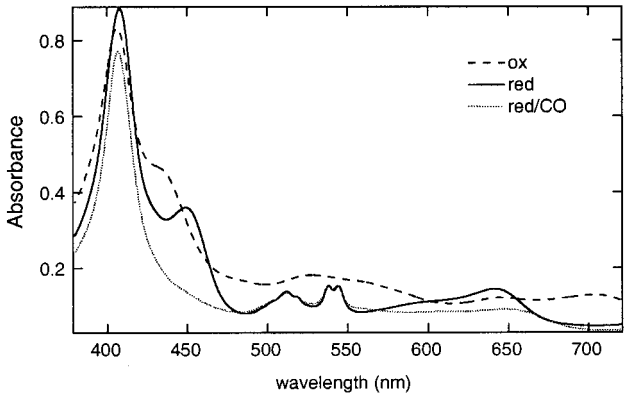


FIGURE 2: Electronic absorption spectra of cytochrome $cd_1$ nitrite reductase from *P. pantotrophus* under various conditions. The different traces represent the spectra of the oxidized (- - -), reduced (—), and carbon monoxide complex of the reduced enzyme (···). Conditions: 10 $\mu$M enzyme, 50 mM potassium phosphate, pH 7.0, 1 mM ascorbate (reduced), 5 $\mu$M phenazine methosulfate (reduced), or 1 mM CO (reduced CO complex), and 20 °C.

Table 2: Rate Constants for the Rearrangements and CO Recombination after Flash Photolysis of the NiR−CO Complex at Different pHs

| pH | rearrangement phase 1 ($s^{-1}$) | rearrangement phase 2 ($s^{-1}$) |
|---|---|---|
| 5.5 | 16 000 | 1700 |
| 7.0 | 19 000 | 3200 |
| 7.5 | 19 000 | 4300 |
| 8.0 | 22 000 | 4500 |
| 8.5 | 17 000 | 2500 |

observed after dissociation of CO (Figure 3A). While the faster of the two phases displayed the same rate within experimental error in the pH range of 5.5−8.5, the slower phase displayed a maximum rate at pH ∼7.5−8.0 (Table 2). Figure 3C shows a kinetic difference spectrum of the rapid rearrangement. At several wavelengths (660, 620, 605, and 400 nm), the amplitudes of the CO dissociation and the rearrangements have the opposite amplitude signs which means that they represent different events. About 70% of the absorbance change is associated with the second rearrangement step. No light-induced absorbance changes were observed following pulsed illumination of the oxidized or unligated reduced enzyme.

*Thermal Dissociation of CO.* Reduced cytochrome $cd_1$ reacts rapidly with $O_2$ and becomes oxidized. When mixing the enzyme−CO complex with an $O_2$-saturated solution, the rate of reaction of the enzyme with $O_2$ was found to be limited by the dissociation of the CO ligand. The rate of thermal dissociation of CO from heme $d_1$ ($k_{off}$) was measured by monitoring absorbance changes at 460 nm following mixing the cytochrome $cd_1$−CO complex with a solution containing $O_2$ in a stopped-flow apparatus at 20 °C (Figure 4). The rate constant was found to be 1.0 ± 0.1 $s^{-1}$ (SD of three measurements).

From the CO recombination and thermal dissociation rates, a dissociation constant ($K_d$) for the cytochrome $cd_1$−CO complex was calculated:

$$K_d = k_{off}/k_{on} = 1\ s^{-1}/13\ mM^{-1}\ s^{-1} \cong 80\ \mu M \quad (2)$$

This $K_d$ value is about 10 times larger than that of the *Ps. aeruginosa* cytochrome $cd_1$ (*17*).

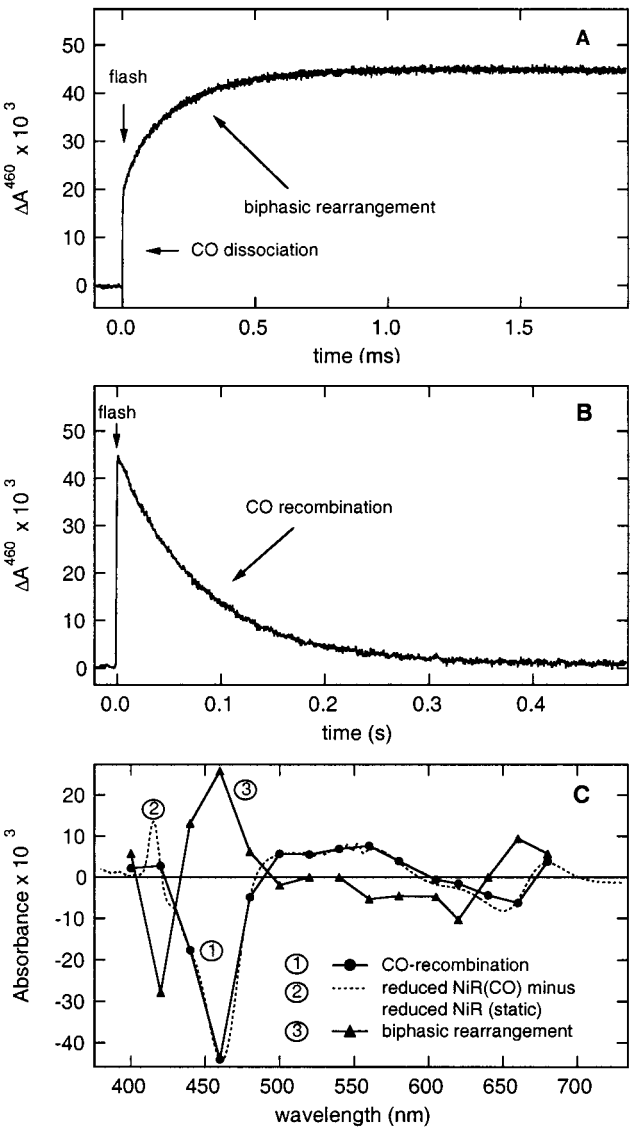


FIGURE 3: Flash photolysis of carbon monoxide from the reduced NiR−CO complex. The rapid increase in absorbance at 460 nm (time zero) is associated with CO dissociation (A and B). The dissociation is followed by a biphasic increase in absorbance with rate constants of (2.2 ± 0.7) × $10^4$ and (4.0 ± 0.1) × $10^3$ $s^{-1}$ at pH 8.0 and 20 °C (A). Recombination of CO with the enzyme is much slower (B), and at 1 mM CO and pH 7, the CO recombination rate ($k_{on}$) was 12 ± 1 $s^{-1}$. The second-order rate constant of the CO recombination was estimated to be 1.3 × $10^4$ $M^{-1}$ $s^{-1}$. This rate was essentially independent of pH in the range of 5.5−8.5 (13 ± 2 $s^{-1}$). Curve 1 in panel C shows the kinetic difference spectrum[2] observed during the recombination of CO with reduced cytochrome $cd_1$. Curve 2 shows the static difference spectrum between the reduced NiR−CO complex and reduced NiR. Curve 3 shows the kinetic difference spectrum of the rapid biphasic rearrangements depicted in panel A. Both phases exhibited the same kinetic difference spectra, and the data depicted in curve 3 represent the sum of the two phases. Conditions: 2.2 $\mu$M active enzyme, 50 mM Tris-HCl, pH 8.0, 2 mM ascorbate, 5 $\mu$M phenazine methosulfate, 1 mM CO, and 20 °C.

*Proton Uptake upon CO Dissociation.* To investigate changes in the protonation state of the enzyme upon CO dissociation, a pH-indicator dye was added to a buffer-free enzyme solution and flash-induced absorbance changes were monitored following CO dissociation. Figure 5A shows absorbance changes at 580 nm of the pH-indicator dye cresol red at pH 8.5 after dissociation of CO. To extract the

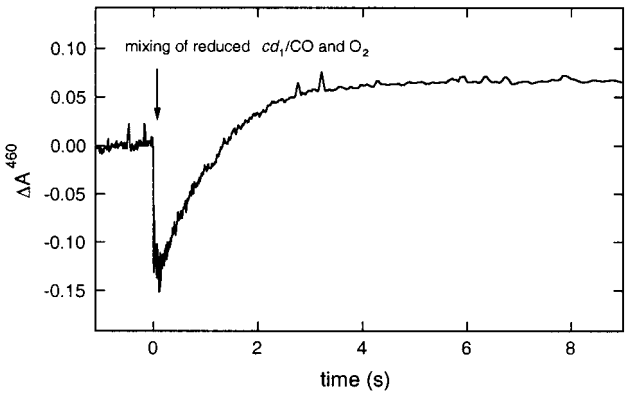


FIGURE 4: Absorbance changes associated with reaction of the reduced NiR−CO complex with an $O_2$-saturated solution after mixing in a stopped-flow apparatus. The oxidation rate of the enzyme was assumed to be limited by the CO dissociation. Consequently, the kinetics of the observed absorbance changes reflects the CO dissociation rate. Conditions after mixing: 0.3 $\mu$M enzyme, 1 mM CO, 1 mM $O_2$, 50 mM potassium phosphate, pH 7.0, and 20 °C.

absorbance changes associated exclusively with alterations in the protonation state of the enzyme, absorbance changes measured in a buffered enzyme solution at the same pH were subtracted from those measured with the buffer-free solution. As shown in Figure 5B, after CO dissociation, we observed uptake of protons with a rate constant of about 1300 $s^{-1}$ at pH 8.5. This value is comparable to the rate constant (within experimental error) of the slower of the two rearrangement phases (Table 2). It was followed by release of protons with a rate constant of 14 ± 3 $s^{-1}$, i.e., the same rate as that of CO recombination (∼13 $s^{-1}$). As seen in Figure 5B, a lag phase was observed before the 1300 $s^{-1}$ phase, which indicates that the event with a rate constant of $1.7 \times 10^4$ $s^{-1}$ (pH 8.5, Table 2) precedes the proton uptake after CO dissociation. The number of protons taken up upon CO dissociation was estimated to be about 0.5 per cytochrome $cd_1$ monomer at both pH 7.5 and 8.5. We also observed the same pH dependence of the rate constant for the proton uptake as for the slower rearrangement phase (see above).

## DISCUSSION

In this study, we have investigated dynamic events linked with the photodissociation and subsequent recombination of CO in reduced cytochrome $cd_1$ from *P. pantotrophus*. We have also determined the crystal structure of the enzyme−CO complex.

In our solution studies, a rapid biphasic absorbance change was observed immediately after flash photolysis of the cytochrome $cd_1$−CO complex (Figure 3A). Both phases displayed the same kinetic difference spectrum (Figure 3C), which indicates that they were associated with the same electronic event at the chromophore. The spectra also indicate that this chromophore is heme $d_1$. An unexpected result of these studies was that the dissociation of the neutral CO ligand was followed by proton uptake and the CO recombination was associated with proton release (Figure 5). Only the slower of the two rearrangement phases was associated with proton uptake from solution. A possible explanation for this behavior is that both kinetic phases were linked to the same proton transfer event at the chromophore; however, the faster phase was associated with a rapid internal proton transfer, while the second, slower phase was limited by the rate of feeding protons from the solvent outside the protein to the internal proton donor.

The X-ray structure of the reduced NiR−CO complex shows CO bound to the iron of the $d_1$ heme in an almost perpendicular orientation relative to the plane of the heme (Figure 1A). The catalytic site is in a relatively polar

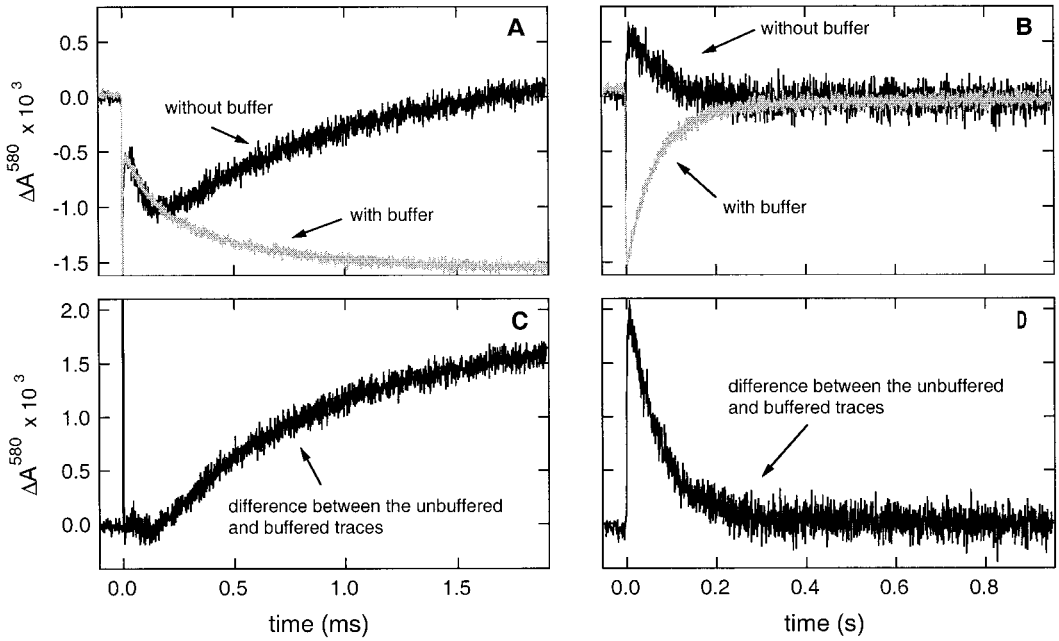


FIGURE 5: Time courses from flash photolysis experiments in the presence of cresol red. Absorbance changes at 580 nm of the pH-indicator dye cresol red show proton uptake following photodissociation (A) and proton release accompanying recombination of CO with reduced cytochrome $cd_1$ (B). To extract changes associated exclusively with proton uptake and release, in panles C and D we show the difference of the absorbance changes of the unbuffered and buffered traces on two different time scales. The buffer capacity of the solution was determined as described in Materials and Methods. Experimental conditions: ∼1 $\mu$M cytochrome $cd_1$, 1 mM ascorbate, 5 $\mu$M phenazine methosulfate, 36 $\mu$M cresol red, 0.1 M KCl, and pH 8.5. The buffered traces were recorded in the presence of 10 mM Tris-HCl at pH 8.5.

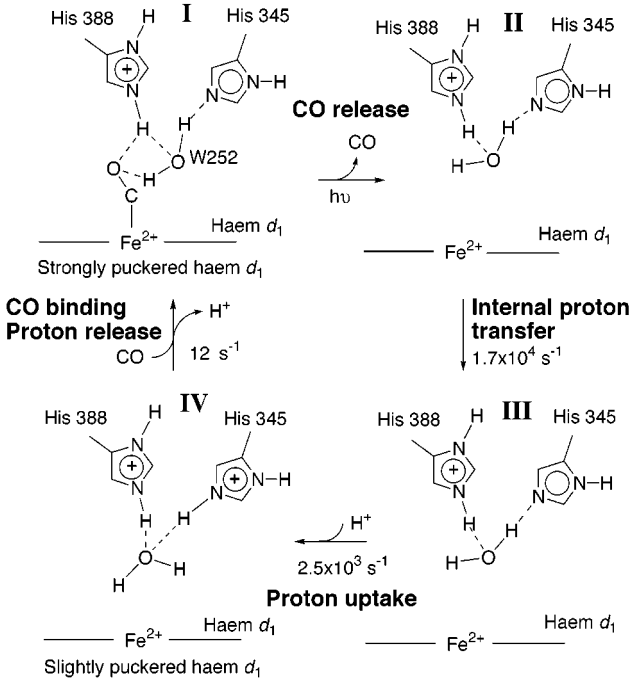


FIGURE 6: Proposed mechanism for proton uptake and proton release following flash photolysis of the reduced $cd_1$−CO complex. Structure **I** corresponds to the reduced NiR−CO complex (Figure 1A). The 532 nm laser flash creates a transient structure (**II**) from which CO has left. This structure undergoes a biphasic process characterized by rapid absorbance changes with rate constants of about $1.7 \times 10^4$ and $2.5 \times 10^3$ $s^{-1}$ (at pH 8.5). The faster of the two phases is probably due to a movement of the water molecule (W252) closer to the now empty sixth ligation site of the heme iron (**III**). This phase may also be correlated with an internal proton transfer. Subsequently, His345 becomes (partly) protonated, and the hydrogen-bonding pattern of the active site is altered (**IV**). Structure **IV** corresponds to the structure of the reduced enzyme (ref *6* and Figure 1D). Recombination of CO with the reduced enzyme returns the system to structure **I**. This process is accompanied by the release of a proton.

environment, and the energy required to introduce or remove a charge in this region is likely to be moderate. Comparison of the structure of the reduced enzyme with the structure of the enzyme−CO complex shows the $d_1$ heme is more puckered when CO is bound to the iron, and a rearrangement of the hydrogen bonding network in the active site takes place. The puckering is also likely to affect the absorbance spectrum of the heme, causing changes in absorbance during the fast rearrangements that we observe. This rearrangement produces an ordered chain of solvent molecules, leading from the active site to the surface of the enzyme−CO complex (Figure 1B). No such chain is visible in the unliganded reduced enzyme at 2.0 Å resolution (*6*). The presence of CO in the active site and the larger puckering of the $d_1$ heme affect the positions of water 252 (W252 in Figure 1A) between His345 and His388 above the distal face of the $d_1$ heme. The ordered chain of water molecules observed in the enzyme−CO complex is linked to W252, which in turn is linked to these histidines. His345 and His388 have previously been implicated as possible proton acceptors or donors during catalysis and ligand binding in the substrate-binding pocket (*4*, *6*). Quantum chemical calculations on a model of the heme $d_1$ pocket (*32*) suggest that the most stable structure for the unliganded reduced enzyme is the one in which His388 and His345 are both protonated. The calculations also indicate that the p*K*s of these histidines change differently with the introduction of ligands or electrons to the active site. Forinstance, when NO is bound to the oxidized heme $d_1$ (ref *6* and Figure 1C), the most stable structure is obtained when His388 is protonated and His345 deprotonated (*32*).

Figure 6 shows a model for events leading to proton uptake and release as a result of photodissociation. The model is based on the three-dimensional structures of reduced NiR (Figure 1D and ref *6*) and the reduced NiR−CO complex (Figure 1A,B). It incorporates results of the present solution studies and also results from quantum chemical calculations (*32*). According to this model, in the unliganded reduced enzyme, both His388 and His345 are protonated. CO binding changes the puckering of heme $d_1$ and the H-bonding network. We assume that these changes lead to a preferential deprotonation of His345 while His388 remains protonated. Upon release of CO, the water molecule in the $d_1$ heme pocket (W252, Figure 1A) moves toward the position seen in the structure of the reduced NiR (Figure 1D) and His345 becomes protonated again.

From the CO dissociation ($k_{off}$) and CO recombination ($k_{on}$) rates, the dissociation constant for the cytochrome $cd_1$−CO complex was calculated to be ~80 $\mu$M. This value is about 1 order of magnitude larger than that for CO binding to the *Ps. aeruginosa* enzyme (*17*) and 2 orders of magnitude larger than that for CO binding to cytochrome *c* oxidase from bovine heart (*27*, *28*). The larger CO dissociation constants of cytochromes $cd_1$ may reflect the fact that these enzymes have evolved to release an otherwise tightly binding reaction product, nitric oxide, from the active site heme iron during catalysis. The CO recombination rate with the reduced heme $d_1$ is slow compared to the rate constants for binding of substrates $NO_2^-$ and $O_2$.

This study on CO release may offer certain insights into the mechanism of NO release during catalysis. Nitric oxide is formed upon one-electron reduction of $NO_2^-$ in the catalytic site of reduced cytochrome $cd_1$:

$$c^{2+}d_1{}^{2+}(NO_2^-) + 2H^+ \rightarrow c^{2+}d_1{}^{3+}(NO) + H_2O \quad (3)$$

His345 and His388 are thought to play an important role in nitrite reduction, first by orienting the substrate by donating hydrogen bonds to one of the oxygens of nitrite in the enzyme−substrate complex and second by binding the product water as hydrogen bond acceptors in the enzyme−product complex (*4*, *6*, *32*). Results described in this paper show, for what we believe is the first time, that proton release and proton uptake take place during the binding and release of a neutral ligand (CO) at the $d_1$ heme. This process changes the overall charge of the protein as a function of the ligation state of the $d_1$ heme. Such a process could modulate the redox potential of the active site and may offer a means for controlling electron transfer between the two different heme centers in the enzyme. To avoid product inhibition during catalysis through the formation of a stable heme $d_1$ $Fe^{2+}$−NO complex (*29*), release of the NO product from the active site must precede electron transfer from heme *c* to heme $d_1$. If NO release from the enzyme−NO complex (Figure 1C) is accompanied by a proton uptake in a manner similar to the release of CO, then such a mechanism may ensure preferential electron transfer to an empty $d_1$ heme and not

to the enzyme−product complex. Proton uptake and release upon the binding of a neutral ligand may also play a controlling function in other proteins.

## ACKNOWLEDGMENT

We thank Prof. S. J. Ferguson and Drs. G. Ranghino and P. A. Williams for discussions. We also thank Lars Nordvall and Christer Andersson for technical support. The ESRF (ID14 EH3) is greatly acknowledged for beam time allocation.

## REFERENCES

1. Zumft, W. G. (1997) *Microbiol. Mol. Biol. Rev. 61*, 533−616.
2. Ferguson, S. J. (1998) *Curr. Opin. Chem. Biol. 2*, 182−193.
3. Rainey, F. A., Kelly, D. P., Stackebrandt, E., Burghardt, J., Hiraishi, A., Katayama, Y., and Wood, A. P. (1999) *Int. J. Syst. Bacteriol. 49* (Part 2), 645−651.
4. Fülöp, V., Moir, J. W., Ferguson, S. J., and Hajdu, J. (1995) *Cell 81*, 369−377.
5. Baker, S. C., Saunders, N. F., Willis, A. C., Ferguson, S. J., Hajdu, J., and Fülöp, V. (1997) *J. Mol. Biol. 269*, 440−455.
6. Williams, P. A., Fülöp, V., Garman, E. F., Saunders, N. F., Ferguson, S. J., and Hajdu, J. (1997) *Nature 389*, 406−412.
7. Moir, J. W., Baratta, D., Richardson, D. J., and Ferguson, S. J. (1993) *Eur. J. Biochem. 212*, 377−385.
8. Williams, P. A., Fülöp, V., Leung, Y. C., Chan, C., Moir, J. W., Howlett, G., Ferguson, S. J., Radford, S. E., and Hajdu, J. (1995) *Nat. Struct. Biol. 2*, 975−982.
9. Parr, S. R., Wilson, M. T., and Greenwood, C. (1975) *Biochem. J. 151*, 51−59.
10. Greenwood, C., Barber, D., Parr, S. R., Antonini, E., Brunori, M., and Colosimo, A. (1978) *Biochem. J. 173*, 11−17.
11. Silvestrini, M. C., Tordi, M. G., Musci, G., and Brunori, M. (1990) *J. Biol. Chem. 265*, 11783−11787.
12. Silvestrini, M. C., Falcinelli, S., Ciabatti, I., Cutruzzola, F., and Brunori, M. (1994) *Biochimie 76*, 641−654.
13. Kobayashi, K., Koppenhofer, A., Ferguson, S. J., and Tagawa, S. (1997) *Biochemistry 36*, 13611−13616.
14. Cheesman, M. R., Ferguson, S. J., Moir, J. W., Richardson, D. J., Zumft, W. G., and Thomson, A. J. (1997) *Biochemistry 36*, 16267−16276.
15. Nurizzo, D., Silvestrini, M. C., Mathieu, M., Cutruzzola, F., Bourgeois, D., Fülöp, V., Hajdu, J., Brunori, M., Tegoni, M., and Cambillau, C. (1997) *Structure 5*, 1157−1171.
16. Cutruzzola, F., Arese, M., Grasso, S., Bellelli, A., and Brunori, M. (1997) *FEBS Lett. 412*, 365−369.
17. Wilson, E. K., Bellelli, A., Liberti, S., Arese, M., Grasso, S., Cutruzzola, F., Brunori, M., and Brzezinski, P. (1999) *Biochemistry 38*, 7556−7564.
18. Ädelroth, P., Ek, M. S., Mitchell, D. M., Gennis, R. B., and Brzezinski, P. (1997) *Biochemistry 36*, 13824−13829.
19. Ädelroth, P., Ek, M., and Brzezinski, P. (1998) *Biochim. Biophys. Acta 1367*, 107−117.
20. Koppenhöfer, A. (1998) Functional studies on the cytochrome-type nitrite reductase from *Thiosphaera pantotropha*, D.Phil. Thesis, University of Oxford, Oxford, U.K.
21. Fülöp, V., Moir, J. W., Ferguson, S. J., and Hajdu, J. (1993) *J. Mol. Biol. 232*, 1211−1212.
22. Murshudov, G. N., Vagin, A. A., and Dodson, E. J. (1997) *Acta Crystallogr. D53*, 240−255.
23. Jones, T. A., and Kjeldgaard, M. O. (1997) *Methods Enzymol. 277*, 173−208.
24. Peng, S. M., and Ibers, J. A. (1976) *J. Am. Chem. Soc. 98*, 8032−8036.
25. Scheidt, W. R., Haller, K. J., Fons, M., Mashiko, T., and Reed, C. A. (1981) *Biochemistry 20*, 3653−3657.
26. Ghosh, A., and Bocian, D. F. (1996) *J. Phys. Chem. 100*, 6363−6367.
27. Gibson, Q. H., and Greenwood, C. (1963) *Biochem. J. 86*, 541−554.
28. Yoshikawa, S., Shinzawa-Itoh, K., Nakashima, R., Yaono, R., Yamashita, E., Inoue, N., Yao, M., Fei, M. J., Libeu, C. P., Mizushima, T., Yamaguchi, H., Tomizaki, T., and Tsukihara, T. (1998) *Science 280*, 1723−1729.
29. Sharma, V. S., Traylor, T. G., Gardiner, R., and Mizukami, H. (1987) *Biochemistry 26*, 3837−3843.
30. Kraulis, P. J. (1991) *J. Appl. Crystallogr. 24*, 946−950.
31. Merrit, E. A., and Murphy, M. E. P. (1994) *Acta Crystallogr. D50*, 869−873.
32. Ranghino, G., Scorza, E., Sjögren, T., Williams, P. A., Ricci, M., and Hajdu, J. (2000) *Biochemistry 39*, 10958−10966.

BI000179Q